ANALYSIS OF CROSS-SPECTRUM SUPERCELLS DURING THE NORTH GEORGIA TORNADO EVENT OF 2 JANUARY 2006

Trisha D. Palmer
Lans P. Rothfusz
Steven E. Nelson

NOAA/National Weather Service
Weather Forecast Office Atlanta,
Peachtree City, Georgia

Brandon A. Miller*

Georgia Institute of Technology
Atlanta, Georgia

Abstract

During the afternoon and evening hours of 2 January 2006, six tornadoes were spawned across portions of north and central Georgia. Observations indicated that mesoscale features were critical in developing and maintaining the near-storm environment, and that cell mergers and/or interactions were precursors to tornadogenesis in every case. The near-storm environment of this event was unique, characterized by an area of eroding cold-air damming in northeast Georgia, and a dryline approaching the state from Alabama. Research on drylines in the Southeast is difficult to find, and anecdotal evidence indicates that drylines such as the one associated with these tornadoes are truly rare events. Rarer still are the supercells that formed along the dryline, in that most supercells in the Southeast are high-precipitation types, yet one of the six tornado-spawning supercells was classic, and another was a low-precipitation supercell. This study focused on the cell mergers and interactions as well as the cross-spectrum nature of these two supercells that produced the strongest tornadoes of the day, an F2 and F3 on the legacy Fujita scale, and how they were influenced by the near-storm environment.

Corresponding Author: Trisha Palmer
National Weather Service
4 Falcon Drive, Peachtree City, Georgia 30269
Email: trisha.palmer@noaa.gov

** Current affiliation: CNN International, Atlanta, GA*

1. Introduction

Classifying supercells based on the amount and spatial distribution of precipitation has been a common practice in both the research and operational fields of meteorology for many years (Doswell et al. 1990, hereafter referred to as D90; Doswell and Burgess 1993, hereafter referred to as D&B93). The common supercell classifications are low-precipitation (LP), classic (CL), and high-precipitation (HP) (D90), although operationally-observed supercells range across the supercell spectrum. While attempting to place any given storm into one of these categories can be difficult, it is important to do so, especially in an operational environment, as each type carries with it a certain set of attendant weather phenomena. Class distinctions are not often obvious in the real atmosphere and events sometimes exist somewhere in between the aforementioned classes, or even evolve from one type to another within the storm's lifecycle (D&B93; Bluestein and Woodall 1990). The most common type of supercell observed is the HP (Johns et al. 1993), especially east of the Mississippi river (D&B93). A vast majority of the rest of the supercells found in the eastern United States can be classified as the CL type, especially those associated with strong tornadoes (D&B93). LP supercells are often associated with the western portions of the Great Plains due to the frequent presence of a surface dryline, which is virtually a necessity for the environment of these storms (Bluestein and Parks 1983; Moller et al. 1994). Since drylines rarely propagate east of the Mississippi River, LP supercells are extremely rare occurrences in the southeastern United States. LP supercells are rarely tornadic, and usually only become so if their structure evolves to become more CL in nature (D&B93).

On the afternoon of 2 January 2006, several supercells formed in Georgia which spanned the spectrum of supercell classifications (Fig. 1). [Note: Additional information on the event, including damage pictures and radar loops, is available online at: www.srh.noaa.gov/ffc/html/tor010206b.shtml.] Though the storms of interest formed in a small spatial area (approximately 50 km apart), they displayed vastly different characteristics throughout their life cycles. The unique character of the storms can be attributed to the variety of mesoscale influences in the near-storm environment. The storms formed along a dryline that propagated eastward across Alabama during the day. Meanwhile, much of northeastern Georgia was in an area of cold-air damming (CAD) (Bell and Bosart 1988), with a majority of the severe weather taking place just south of the intersection of these two boundaries (Fig. 2). The purpose of this paper is twofold: (1) describe the cross-spectrum nature of two of the supercells from 2 January 2006, Supercell 1 (S1) and Supercell 8 (S8); and (2) discuss the important observation that each of the six tornadoes from this event was the result of a storm merger or cell interaction.

Supercell S1 (Fig. 1) was the northernmost supercell to form along the dryline, and the closest to the CAD "wedge" front. It produced hail 2 in (over 5 cm) in diameter, as well as an F2 (strong) tornado on the legacy Fujita scale leaving a path just over 11 km long and 1.5 km wide in the communities of Palmetto (Fulton County) and Tyrone (Fayette County). The storm followed a lifecycle similar to an archetypal Great Plains CL supercell (D90).

Supercell S8 (Fig. 1) formed approximately 48 km south of S1 and was slightly ahead of the main line of storms. It produced the strongest tornado of the day – an F3 which moved a house over 18 m from its foundation and tossed two vehicles almost 230 m near the community of Hollonville (northwest Pike County). The path of this significant tornado was 4.8 km long and 1.5 km wide. As will be shown later in the paper, S8 displayed LP characteristics during the first part of its lifecycle, later becoming classic and eventually HP in nature (D90; D&B93).

2. Synoptic Environment

A progressive long-wave pattern was in place over the continental United States (CONUS) during the week leading up to the event, with four upper-level (300 mb) troughs moving through the southeastern United States during the period from 27 December 2005 through 3 January 2006. The first of these troughs produced nine tornadoes across Georgia on 28 December. A similar pattern was expected on 2 January with a negatively tilted trough at 500 mb centered on a line from Kansas City, Missouri, to Shreveport, Louisiana, at 1200 UTC on 2 January (Fig. 3a). By 0000 UTC on 3 January the trough had increased in negative tilt and was centered on a line from Springfield, Illinois, to Birmingham, Alabama (Fig. 3b). During this time, a short wave moved through the base of the long-wave trough, from near Dallas, Texas, at 1200 UTC 2 January to near Augusta, Georgia, at 0000 UTC 3 January (Fig. 3).

The 250 mb winds at 1200 UTC 2 January 2006 (Fig. 4a) revealed a cyclonically-curved jet spanning the bottom of the negatively-tilted trough. Per the behavior of curved jets (Moore and VanKnowe 1992), rising air exists on the downstream dipole of the trough axis (and subsequently the jet axis). This is because the along-contour component of the ageostrophic wind enhances divergence downstream of the trough and convergence upstream of the trough (Moore and VanKnowe 1992, see their Figs. 1 and 4b). In the case of 2 January 2006, however, the extreme curvature of the trough did not

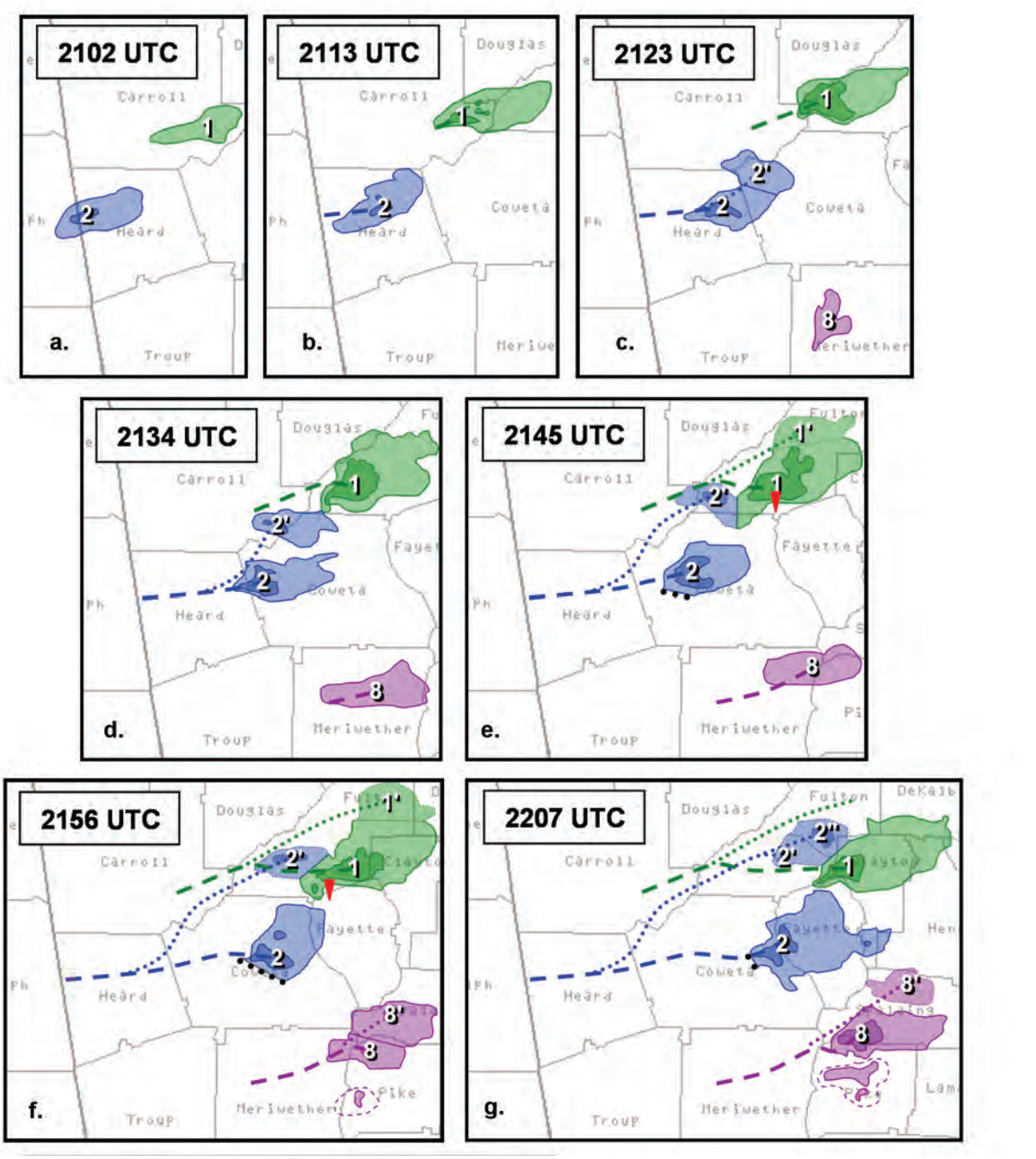

Fig. 1. Schematic of splitting and merging storms and their paths on 2 January 2006. Shaded contours are 30 and 50 dBZ reflectivities. Dashed contours near S8 (f., g., and h.) indicate 20 dBZ shower. Large dots (south edge of S2) indicate adjacent storm reflectivities omitted for figure clarity. Dashed and dotted paths indicate right- and left-moving storm paths, respectively. Bottom point of inverted red triangles (S1 and S8) show approximate tornado locations. Primes (′) indicate storm splits. Labeled storms are numbered non-sequentially to account for additional supercells that occurred during the outbreak but were not included in the figure for clarity.

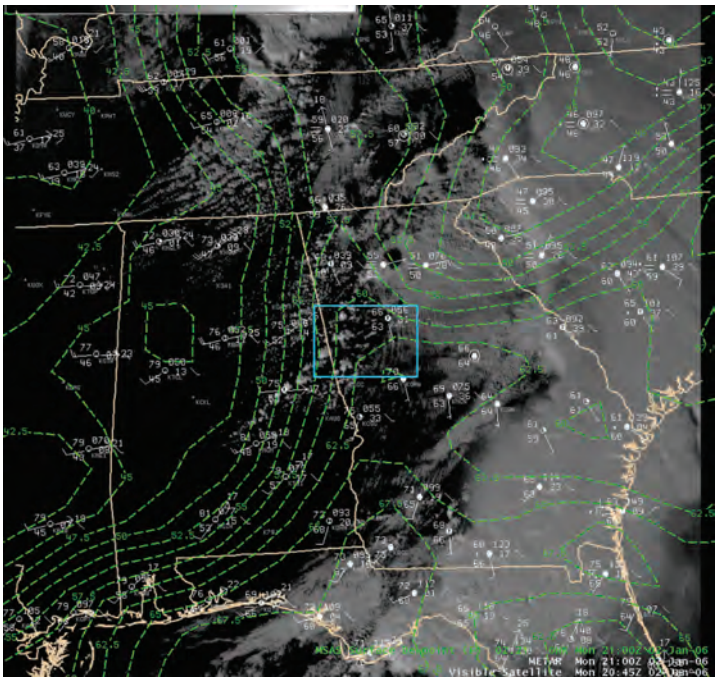

Fig. 2. Surface conditions at 2100 UTC, 2 January 2006, near the time of convective initiation. Included are the GOES visible image at 2045 UTC, overlain with standard surface observations, and dewpoint temperatures (dashed green contours, 2.5°F intervals). Note the cold front from central Tennessee into northwest Mississippi; the dryline in eastern Alabama, and the CAD in northeast Georgia. The cyan box outlines approximately the same area shown in as Fig. 1h.

allow the upstream jet streak to entirely propagate around the cyclonic flow, inducing an ageostrophic flow upstream of the trough; this ageostrophic flow produced upper divergence and subsequent upward motion. Speed divergence existed in the area as well (northern Mississippi/Alabama and western Tennessee), with wind speeds increasing from 75 kt at the base of the trough to 95 kt near the inflection point (Fig. 4a). At 0000 UTC 3 January 2006 (Fig 4b), the speed divergence had increased significantly from 60 kt to 110 kt (Fig. 4b). In addition to the extreme speed divergence aloft, there was also significant mass divergence throughout the Southeast during the period (Figs. 4a and b). This combination of extreme jet-level divergence along with the negatively tilting trough led to significant upward vertical velocities (UVV) over the Southeast, especially in Georgia.

Between 1200 UTC 1 January and 1200 UTC 2 January 2006, a 500 mb low closed off over the lower Missouri Valley. However, like approximately 20% of the cool-season tornadic cases found in Guyer et al. (2006) (hereafter referred to as G06), the Gulf Coast states were beneath or shifted just slightly to the south of the mid-level jet. At this level, while streamline analysis would reveal significant diffluence over the Southeast downstream of the closed mid-level low, speed convergence was noted with wind speeds decreasing from 65 kt at Jackson, Mississippi (KJAN) to 35 kt at Greensboro, North Carolina (KGSO). By 0000 UTC 3 January, during the outbreak but after the most significant tornadoes of the day had occurred, the mid-level jet had shifted south of the primary outbreak area, supportive of the idea that perhaps this was not a "typical" Gulf Coast cool-season tornadic outbreak.

Beginning at 0000 UTC 2 January 2006, significant warm air advection (WAA) existed ahead of the low at 850 mb, especially in Missouri (not shown). The WAA continued east of the low, moving into the Ohio River Valley by 1200 UTC and stretching into the Great Lakes (Fig. 5a). In addition, a 35 to 40 kt southwesterly low-level jet, consistent with the findings of G06, stretched

Fig. 3-a

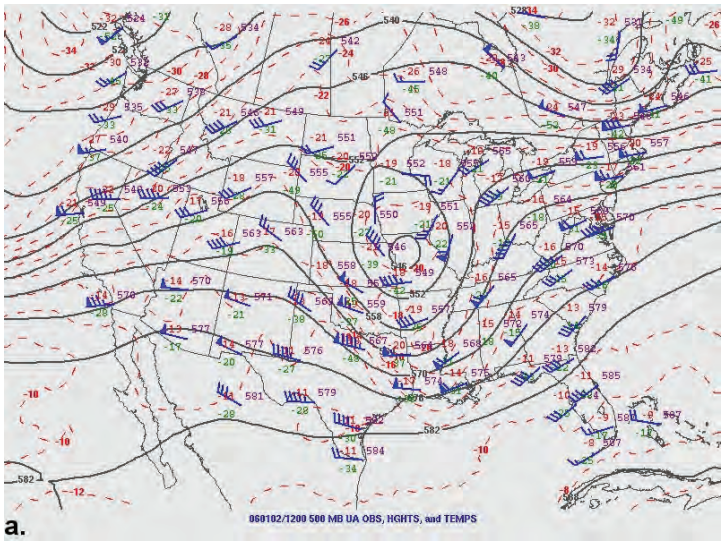

Fig. 3-b

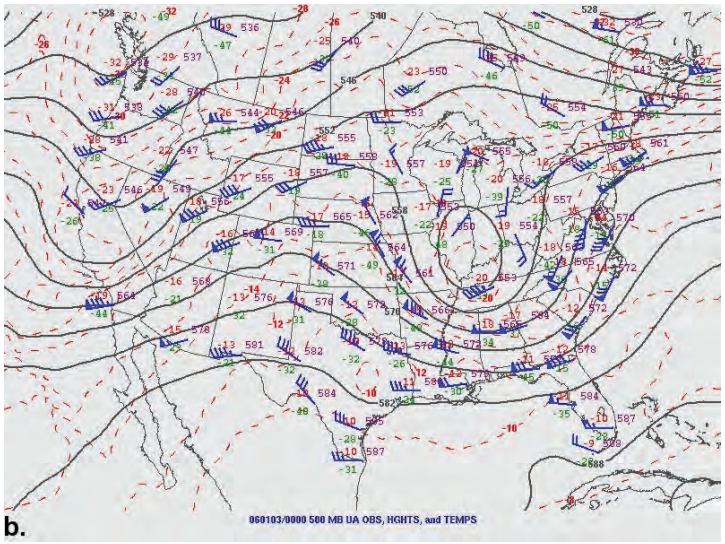

Fig. 3. (a) 500 mb observational surface analysis and station plots for 1200 UTC 2 January 2006. Solid black lines are contours of geopotential heights (every 6 dam) and dashed red lines are contours of temperature (every 2°C). (b) Same as in (a), except for 0000 UTC 3 January 2006 (Source: SPC).

from Louisiana to the Carolinas. By 0000 UTC 3 January 2006 the WAA continued east along the Ohio River and stretched from Georgia to Lake Erie (Fig. 5b). The most significant WAA, destabilizing the atmosphere and contributing to UVV, existed in the Southeast, mainly across Georgia and Tennessee, but also extending into the Ohio River Valley. Consequently, all of the states within these regions experienced severe weather on 2 January, including seven tornadoes in Kentucky (U.S. Department of Commerce 2006).

Geostationary Operational Environmental Satellite (GOES) water vapor imagery for 1200 UTC on 2 January 2006 showed convection occurring across the Southeast early in the day (not shown). This convection played an important role in maintaining the integrity of the CAD, which will be addressed later. By 1900 UTC, the convection had cleared the western half of Georgia with a clear slot opening behind the convection. An area of mid-level moisture "nosed" into the clear slot in northern Alabama between 1500 and 2000 UTC (not shown). Convective initiation (CI) occurred in the clear slot between 1900 and 2000 UTC, approximately 80 km ahead of the mid-level moisture.

Fig. 4-a

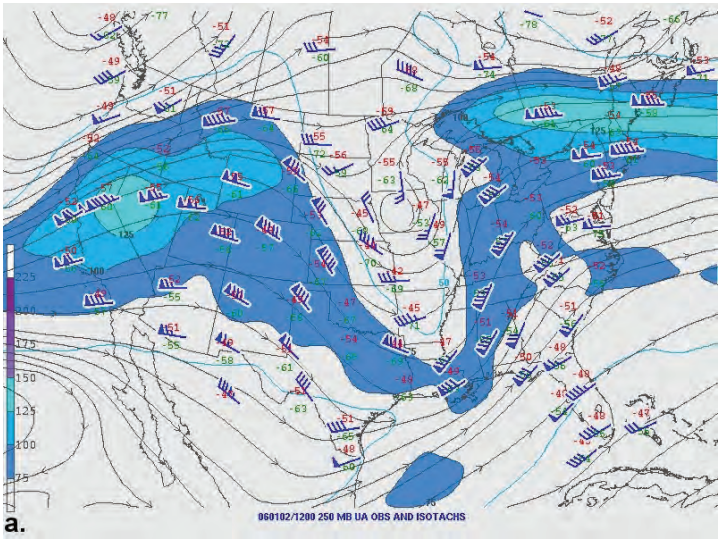

Fig. 4-b

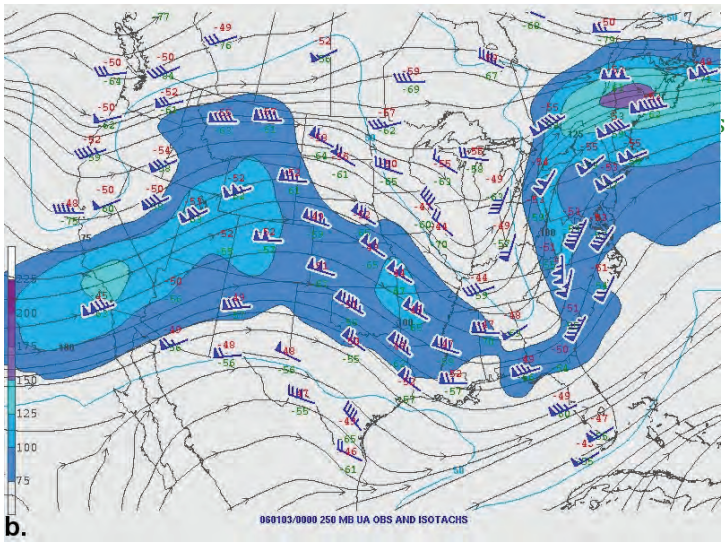

Fig. 4. (a) 250 mb streamline analysis and station plots for 1200 UTC 2 January 2006. Solid blue contours and shading are isotachs (every 25 kt). (b) Same as in (a), except for 0000 UTC 3 January 2006 (Source: SPC).

Fig. 5-a

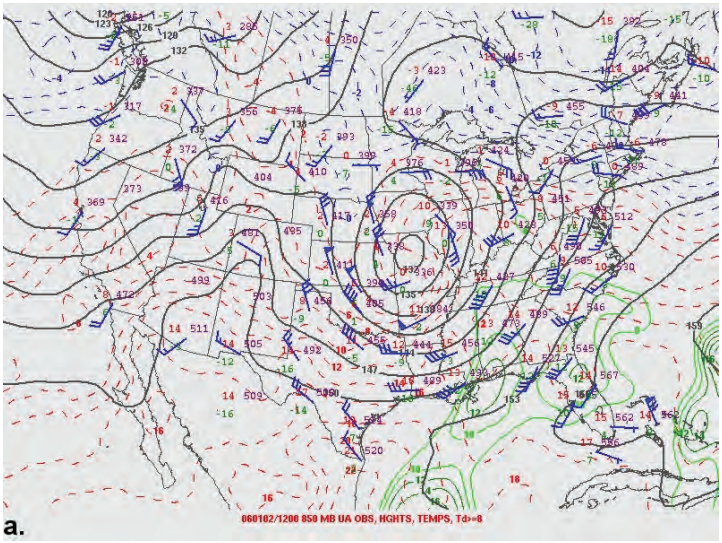

Fig. 5-b

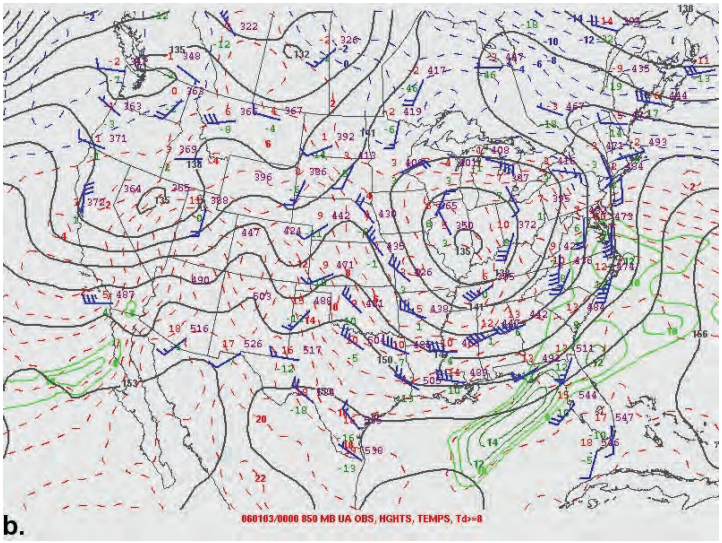

Fig. 5. (a) 850 mb observational surface analysis and station plots for 1200 UTC 2 January 2006. Solid black lines are contours of geopotential heights (every 3 dam), dashed red lines are contours of temperatures (every 1°C), and solid green lines are contours of dewpoint temperature (every 1°C greater than 8°C). (b) Same as in (a), except for 0000 UTC 3 January 2006 (Source: SPC).

3. Mesoscale Environment

a. Dryline

The dryline, recognized as a north-south oriented horizontal moisture gradient traditionally located in the central and southern plains of the United States, is often evaluated by severe thunderstorm forecasters as a prime area for convective development (Rhea 1966). The dryline is normally confined to the western plains, but in rare events, such as on 19 March 2003 (Barbré et al. 2005), the dryline can be intensified and carried eastward during large-scale translating weather events such as low pressure centers (Hane et al. 1993; Hane et al. 2001). This eastward translation of the dryline was the case during the 2 January 2006 tornado event. As the parent low tracked from eastern Colorado across the Missouri River Valley and into the Ohio River Valley from 1200 UTC on 1 January to 0000 UTC on 3 January, the dryline remained approximately 250 km southeast of the surface cold front, the latter of which was in central Tennessee around the time of CI. The dryline and cold front can be seen both in surface analyses and also cloud boundaries in GOES visible satellite images (Fig. 2). During the late morning of 2 January 2006, however, the dryline lost its integrity as it moved from Mississippi into Alabama, but then regained its intensity over eastern Alabama in time for convection to initiate along it, resulting in the severe weather in Georgia. Fig. 6a shows the relatively weak dewpoint gradient over northwest Alabama at 1800 UTC, however, by 2000 UTC, the surface dewpoint gradient intensified in eastern Alabama (Fig. 6b). At 1600 UTC the Automated Surface Observing System (ASOS) station near Birmingham, Alabama (KBHM), had a 62°F dewpoint with a 71°F surface temperature and winds from 240 degrees. At 2000 UTC, after the passage of the dryline, the same station reported a 48°F dewpoint with a surface temperature of 77°F and winds from 250 degrees. Meanwhile, the surface cold front remained approximately 160 km northwest of KBHM at 2000 UTC, marked by a 10°F temperature decrease and 70 degree wind shift. The dryline's passage was also marked in the upper air soundings taken south of Birmingham, Alabama (KBMX), and at Peachtree City, Georgia (KFFC), and can be seen especially in the dry air intrusion aloft (Figs. 7 and 8). The presence of this dryline, as well as its relative increase in intensity, helped to increase moisture convergence and provide sufficient upward vertical motion needed to initiate convection on 2 January 2006.

Fig. 6-a

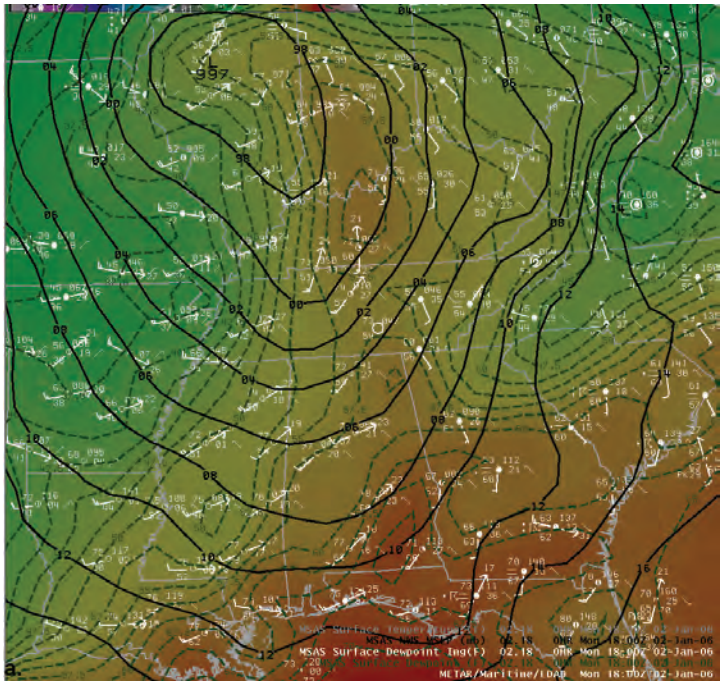

Fig. 6-b

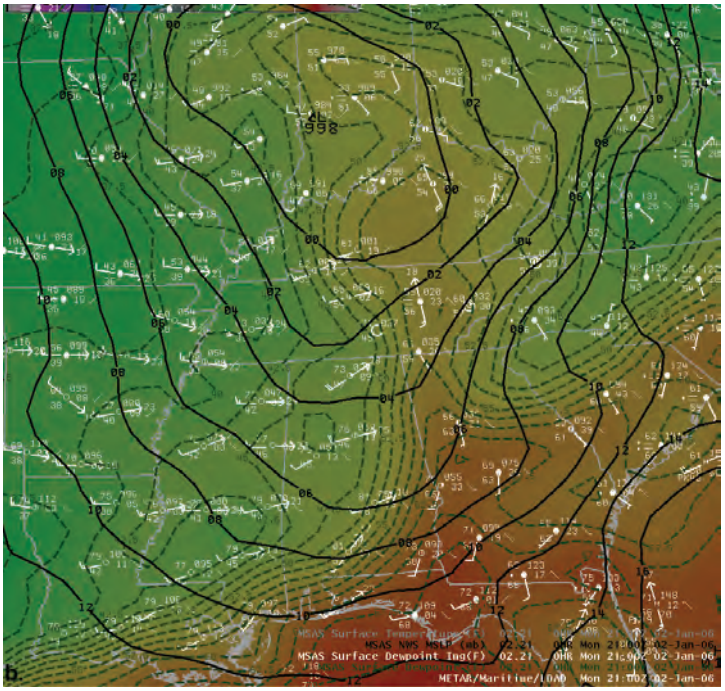

Fig. 6. Standard surface observations, pressures (black contours, 2 mb intervals), and dewpoint temperature analysis (color shading and dashed contours, 2.5°F intervals) from (a) 1800 UTC and (b) 2100 UTC 2 January. Note in (a) the presence of the dewpoint gradient marking the location of the cold front along the Mississippi River; however the dryline's location in Mississippi is difficult to determine. In (b) the dewpoint gradient in the southeast indicates the presence of the dryline, and the cold front is associated with the temperature gradient from oriented east-west from central Tennessee to near central Arkansas.

b. Cold-air damming

Appalachian cold-air damming (CAD) refers to the phenomenon of cold air becoming entrenched along the eastern slopes of Appalachian Mountains through a process of geostrophic adjustment (Richwien 1980; Bell and Bosart 1988). The geostrophic adjustment results in a dome of cool, stable air and is most easily identified by a "U"-shape in the isobars on a sea level pressure map, but can also be seen in a trough of equivalent potential temperature (θ_e) ("U"-shaped as well) against the lee of the mountains. While a full explanation of CAD is beyond the scope of this paper, Lackmann and Stanton (2004) explain that "the relative coldness of the CAD is the result of: (i) along-barrier cold advection, (ii) orographic ascent, and, when sufficient moisture and lift are present; (iii) evaporative cooling and sub-cloud sheltering from insolation." Oftentimes the CAD can be slow to erode and the evaporation of precipitation can act to intensify the cold dome, thus increasing the low-level baroclinicity between the mountains and the coast, leading to an entrenching of the CAD (Bell and Bosart 1988). The front that develops between the CAD and the surrounding airmass resembles quasi-stationary warm fronts that can maintain temperature contrasts of more than 10°C in less than 100 km (Bosart 1975). This front, often termed the "wedge" front or Piedmont front due to its common location over the Piedmont region east of the Appalachian Mountains, can also become a focal point for potentially severe convection (Businger et al. 1991; Vescio et al. 1993).

The CAD scenario in place during the 2 January 2006 event was that of a "hybrid" CAD, in which the central mean sea level pressure of the parent high is less than 1030 mb and diabatic processes contribute to the CAD onset (Bailey et al. 2003). One of the most difficult challenges facing a forecaster in this region is the prediction of cold dome demise (Keeter et al. 1995). CAD erosion takes place when the inversion separating the topographically trapped air from the free atmosphere is mixed out via any of several processes, such as thermal advection, solar heating, a frontal passage, etc. (Lackmann and Stanton 2004). In their research, Bailey et al. (2003) found that CAD erosion was independent of onset mechanism, and although Stanton (2003) and Lackmann and Stanton (2004) only studied the physical mechanisms associated with classical CAD, their findings can be applied to the hybrid CAD during this event. The erosion mechanism influential in the demise of the hybrid CAD in place on 2 January was a "cold frontal passage". During this erosion mechanism, the cold front is influential in the demise of the CAD event, whereas in other erosion scenarios (e.g., "northwestern low"), the CAD has eroded before the front arrives (Stanton 2003). When the erosion mechanism is cold frontal passage, eroding of the cold dome may begin before the surface front passes the damming region, as a result of frontal steepening caused by mountain barrier blocking (Shumacher et al. 1996; Brennan et al. 2003). The erosion occurs because cold advection aloft reaches the damming region, weakens the capping inversion, and

Fig. 7-a

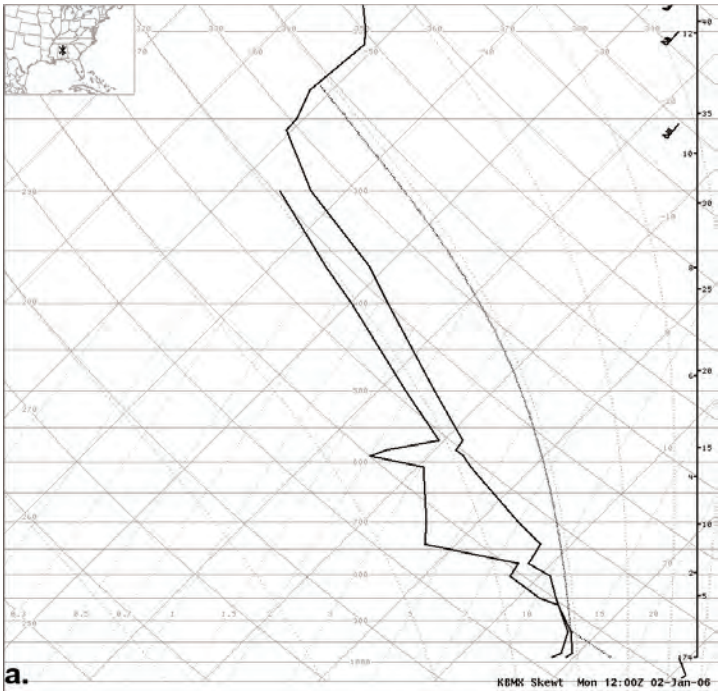

Fig. 7-b

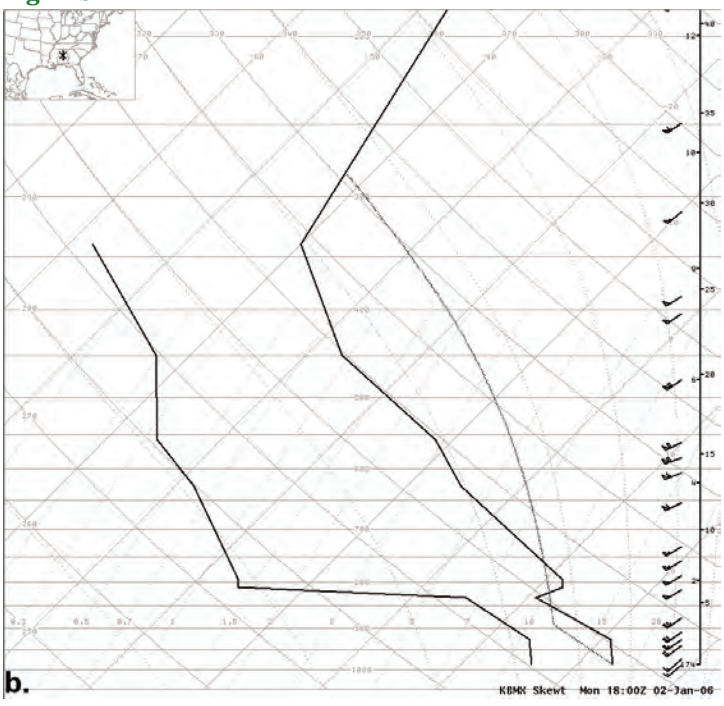

Fig. 7. Upper-air rawinsonde observations from KBMX (Birmingham, Alabama) plotted on a skew-T diagram. (a) 1200 UTC, and (b) 1800 UTC 2 January 2006.

subsidence occurs, leading to drying and dissipation of cloud cover. The lack of cloud cover allows solar heating to begin eroding the CAD before the arrival of the surface front (Lackmann and Stanton 2004).

Fig. 8-a

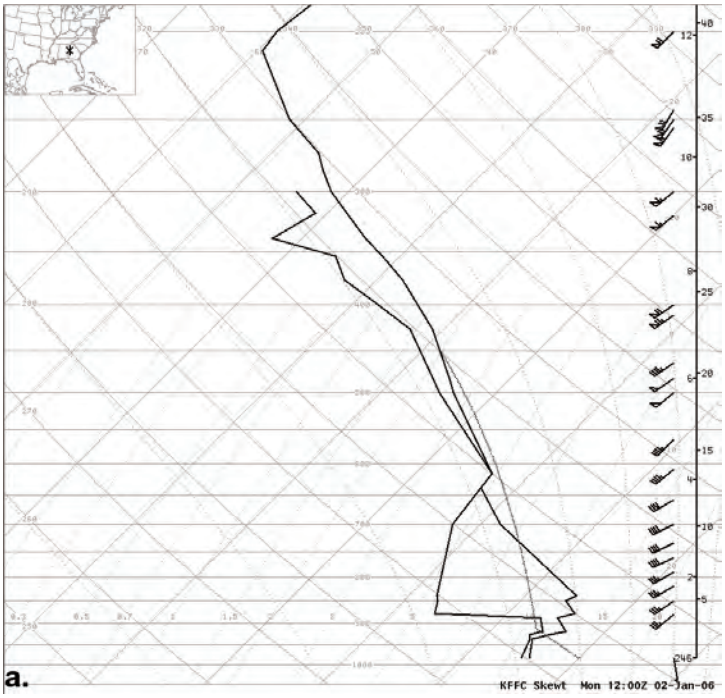

Fig. 8-b

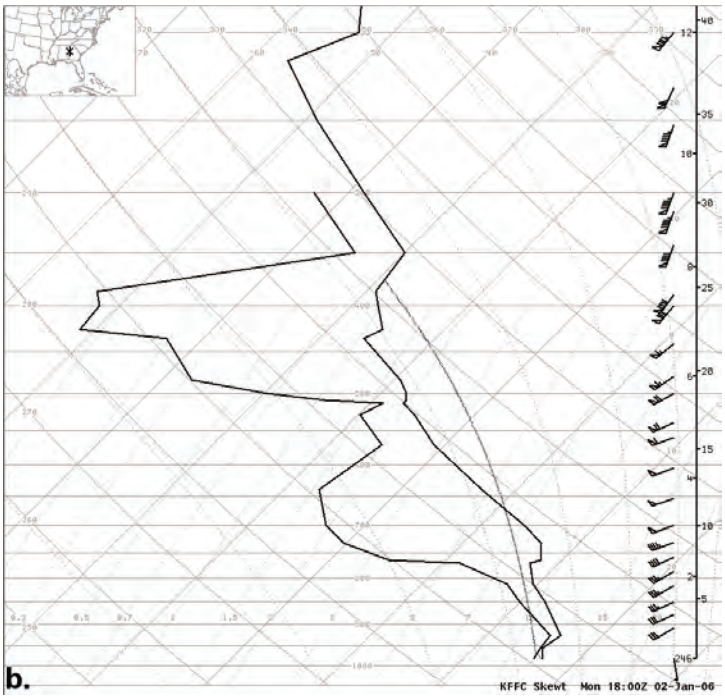

Fig. 8. Upper-air rawinsonde observations from KFFC (Peachtree City, Georgia) plotted on a skew-T diagram. (a) 1200 UTC, (b) 1800 UTC 2 January 2006, and (c) 0000 UTC 3 January 2006.

During the early morning of 2 January 2006, any erosion of the CAD could have significantly influenced the mesoscale environment by weakening the low-level convergence, moisture pooling, and baroclinicity in the area of the wedge front. The eroding was not observed, however, likely due to the morning convection and associated mid- and high-level clouds above a thick low-level stratus layer in the CAD region. This cloud cover (seen in Fig. 2) inhibited the aforementioned diabatic heating to begin eroding the CAD. While it was believed at the time of the event that the morning convection could stabilize the environment via reduced solar insolation and thus decrease the chance for severe weather later in the day, it may have actually played an important role in its eventual occurrence by strengthening the CAD via the very mechanism of reduced insolation over the CAD region. Conversely, cloud cover south of the CAD broke up into cumulus streets in the high θ_e air, allowing the temperatures to warm further (to between 68-77°F, which increased the baroclinicity along and to the south and west of the wedge front. However, the exact role that the CAD and more specifically, the wedge front itself, played in CI or convective enhancement is beyond the scope of this paper.

c. Other mesoscale parameters

The morning convection nearly cleared Alabama completely by 1600 UTC (local noon) (not shown), and provided ample solar heating time for surface temperatures to rise to 80°F (27°C) in southern Alabama. In

Fig. 8-c

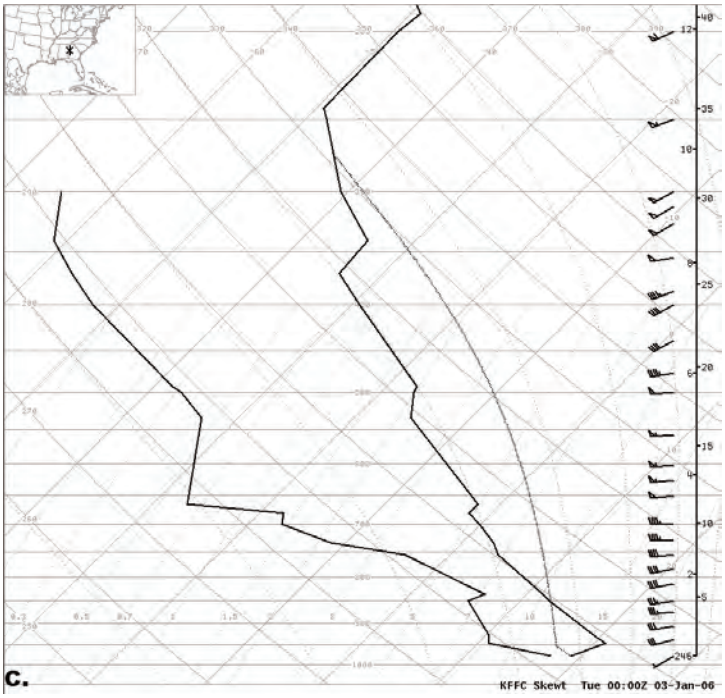

the moisture-rich area ahead of the dryline, mesoanalyses produced by the Storm Prediction Center (SPC) (not shown) showed surface-based Convective Available Potential Energy (SBCAPE) values increased to between 1000 and 2000 J kg^{-1} in eastern Alabama between 1500 and 2000 UTC. 100 mb mixed-layer CAPE (MLCAPE) values were well over 1000 J kg^{-1} in these same areas, consistent with (and perhaps slightly higher than) the findings of G06. Analysis of the 1800 UTC sounding data from KBMX showed a SBCAPE value of 1991 J kg^{-1}, while the KFFC sounding showed SBCAPE of 565 J kg^{-1}, increasing to 1633 J kg^{-1} at 0000 UTC (Figs. 7 and 8). MLCAPE on the aforementioned SPC mesoanalyses near 0000 UTC at the north end of the warm sector, in which KFFC was located, also increased to well over 1000 J kg^{-1} as the moisture-rich environment from eastern Alabama earlier in the afternoon advected to the east. The sounding and mesoanalysis data illustrate how the instability was increasing and spreading eastward in the clear air behind the morning convection. Based on these data, a moderately unstable environment with SBCAPEs approaching 2000 J kg^{-1} and MLCAPEs between 1000 and 1500 J kg^{-1} can be inferred in the location of CI of the storms.

According to Craven et al. (2002), low-level shear (0-1 km) values greater than 15-20 kt (8-10 m s^{-1}) have been associated with significant tornado development in supercells. On the afternoon of 2 January 2006, 0-1 km shear values of approximately 30-40 kt (15-21 m s^{-1}) were located throughout the region of the storm development. These values are in the upper two quartiles associated with F2 and greater tornadoes in Gulf Coast storms, according to G06. Deep layer shear (0-6 km) is another important factor specifically in storm development and sustenance, with values of 35-40 kt and greater associated with supercells (Rasmussen and Blanchard 1998). For 2 January, deep-layer shear values of approximately 60 kt were located in the area of CI. The storms moved into areas of even higher (>70 kt) deep-layer shear after 2300 UTC. From the study done by G06, the large area of 0-6 km shear of greater than 60 kt is in the upper quartile of their climatological database; the area of 70 kt is beyond the 90th percentile of the G06 database. Storm relative helicity (SRH) values between the surface and 1 km (e.g., Davies-Jones et al. 1990) ranged from 300 to 500 m^2 s^{-2} through the afternoon hours on 2 January, mostly in excess of the upper quartile of storms studied by G06. Similarly, 0-3 km SRH also mainly ranged from 300 to 500 m^2 s^{-2}, but surpassed 600 m^2 s^{-2} in parts of northeast Georgia, in the southern reaches of the CAD, which is common in these areas. These SRH values were mainly in the upper one to two quartiles of storms studied by G06. The hodograph provided by the 1800 UTC KFFC sounding (Fig. 9) indicated 239 m^2 s^{-2} of 0-3 km SRH; this was before CI. It can be seen

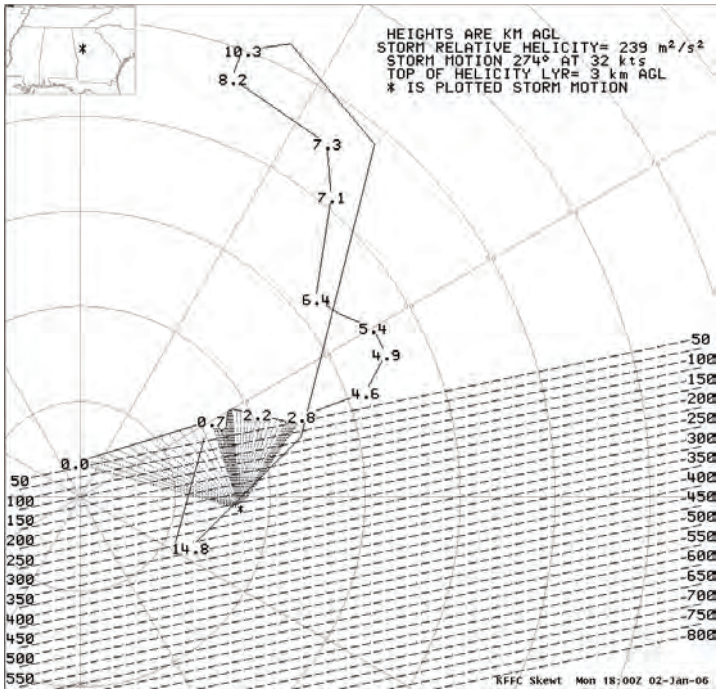

Fig. 9. Hodograph derived from the 1800 UTC upper-air rawinsonde observation from KFFC.

from the 1200 UTC and 1800 UTC KFFC soundings (Figs. 8a and b) that the surface layer warmed as the dryline approached. Because of the increased easterly component of the surface wind due to the proximity of the CAD, shear is typically higher in the stable airmass close to the cold dome. In any situation, to properly evaluate SRH, the hodograph should be modified to use the inflow airmass. However, in this particular case, due to the backed winds ahead of the dryline, using the inflow airmass instead of the 1800 UTC KFFC surface winds would have made negligible difference to the 0-3 km SRH values. [Note: The Advanced Weather Interactive Processing System (AWIPS) Display Two Dimensions (D2D) uses the 30R75 (30° to the right and 75 percent of the 0-6 km density weighted average wind) method to calculate storm motion based on Maddox (1976) and Davies and Johns (1993). There is no way to manually modify the storm motion in D2D.] The significant amount of shear throughout the environment most certainly helped the storms not only to initiate, but also helped the storms to maintain their intensity, even after leaving areas of higher instability.

The abnormally high amounts of shear (both deep-layer and low-level) and helicity associated with this event lead the authors to believe that these storms were certainly not typical of a Gulf Coast outbreak, warm or cool season. This is especially the case when compared with shear values that are typical of cool season outbreaks (i.e., G06), which would normally be associated with high amounts of shear

themselves due to the more southerly extent of the upper-level jet. When compared to other cool-season outbreaks, shear parameters from the 2 January 2006 outbreak were all at least in the upper quartiles of the G06 study, and in some cases beyond the 90th percentile. It seems, in fact, that many of the calculated parameters (e.g., Significant Tornado Parameter; Thompson et al. (2004)) associated with the 2 January 2006 event are more consistent with the findings of Thompson et al. (2004) and Thompson et al. (2003) rather than G06. In the former two, the studies were not limited to any particular geographic region, and indeed included storms in the Plains, many of which likely formed along drylines. It is improbable that any of the G06 storms formed along drylines, possibly explaining the dissimilarity of the 2 January 2006 event to other "typical" cool-season tornadic outbreaks. The presence of the dryline no doubt enhanced the severity and explosive development of the storms, and the mere fact that a dryline developed and propagated across the Southeast provides an indication of the unique nature of this event as a whole.

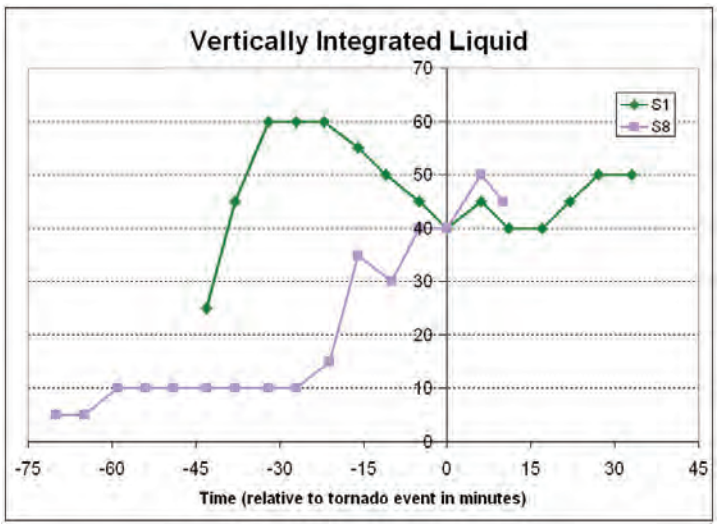

Fig. 10. Vertically integrated liquid (VIL) trends of supercells S1 versus S8, beginning with the first discernable 30+ dBZ echo, with respect to tornado event time. Maximum VIL is the maximum value at that time step from either KFFC or KJGX; with the proximity of these storms to KFFC and the amount of time spent in the "cone of silence" most of these values were obtained from KJGX. Notice the much lower VILs in S8 vs. S1 leading up to tornadogenesis.

4. Storm-scale Analysis

Characteristics of supercells S1 versus S8 as seen from the Weather Surveillance Radar 88 Doppler (WSR-88D) (KFFC) in Peachtree City were vastly different (Figs. 10-14). For comparative purposes, Fig. 10 is a time series of vertically integrated reflectivity (VIL) as computed by the WSR-88D for each storm throughout the storms' lifecycles, relative to the tornado event. This will be discussed further below. While these storms must be evaluated individually before direct comparisons can be made between them, one storm-scale feature that was applicable to all storms that day was the storm motion and behavior: the lowest 4-6 km represented by the straight-line hodograph in Fig. 9 supports splitting storms. This is an important feature that factored into the 2 January 2006 event.

At the beginning of the event, KFFC operated in Volume Coverage Pattern (VCP) 121 due to significant range-folding problems earlier in the day as convection moved through central and southern Georgia. VCP 121 has the same elevation angles as VCP 21 but utilizes the Multiple Pulse Repetition Frequency (PRF) Dealiasing Algorithm (MPDA) to mitigate range-folding (Zittel and Wiegman 2005) by combining velocity data from different PRFs at the lowest five elevation scans. KFFC was switched to VCP 12 at 2218 UTC. KJGX, in Warner Robins (near Macon), Georgia, was kept in VCP 121 throughout the duration of the event to minimize range-folding.

Radar operators noticed during the event that the velocity data for the Pike County storm at the lowest elevation scans from KFFC were extremely "noisy." This can be seen in Figs. 12 and 13 described below. While it is beyond the scope of this paper to explain these radar ambiguities and why rotation was not evident at these altitudes, some hypotheses that have been put forth include the clutter suppression invoked for KFFC and that the storm was an LP supercell with a relatively high cloud base and thus had few scatterers at those low elevation scans below the updraft base.

Finally, the 0.9° data from KFFC somehow did not get archived locally for playback on the Weather Event Simulator (WES), which was used for most of this research. Thus, the authors used archived Level II data on GR2Analyst (Windows-based software for viewing WSR-88D data; more information is available online at http://www.grlevelx.com) for Figs.11-14.

a. Supercell S1

S1 showed all the signs of a classic supercell (D90; D&B93), especially as it evolved into its tornadic phase. For example, the presence of a deep, persistent mesocyclone was noted within 30 minutes of the storm's initiation at approximately 2045 UTC. Other indications of this classic supercellular behavior were deviant rightward motion and a hook echo. The F2 tornado touched down approximately

continued on p. 70

Fig. 11-a

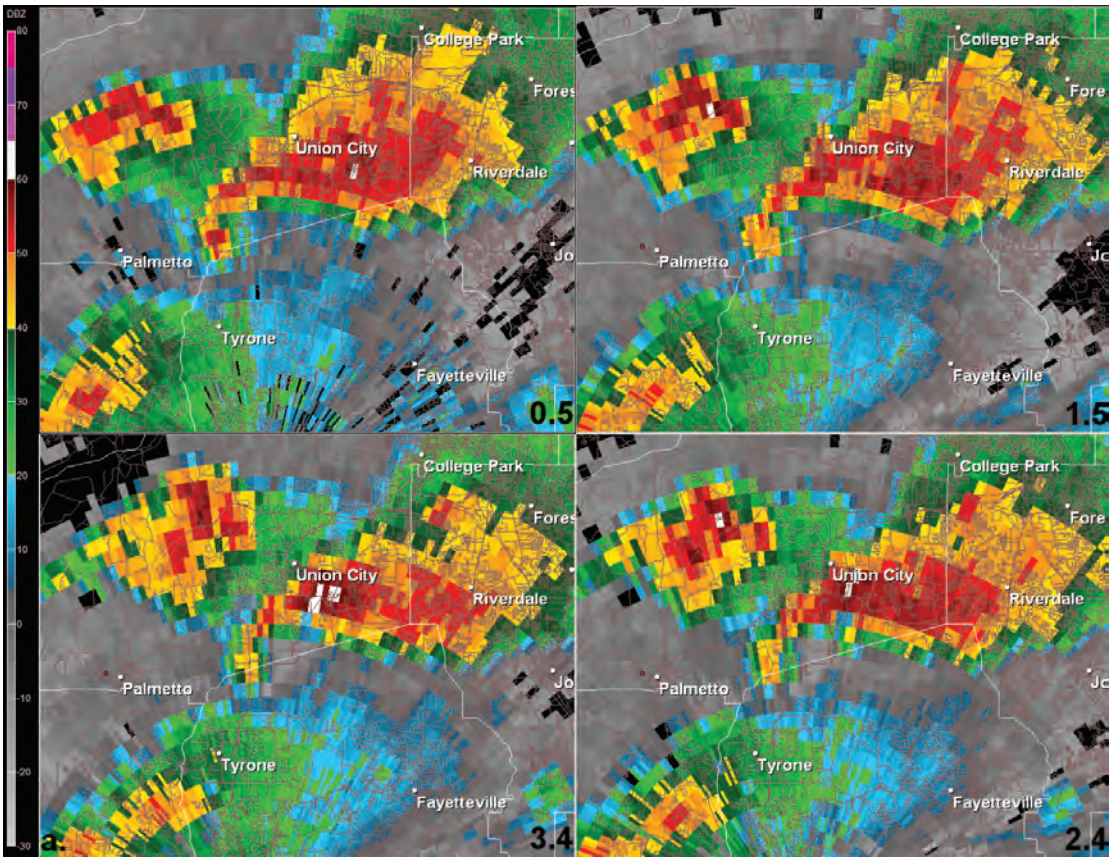

Fig. 11-b

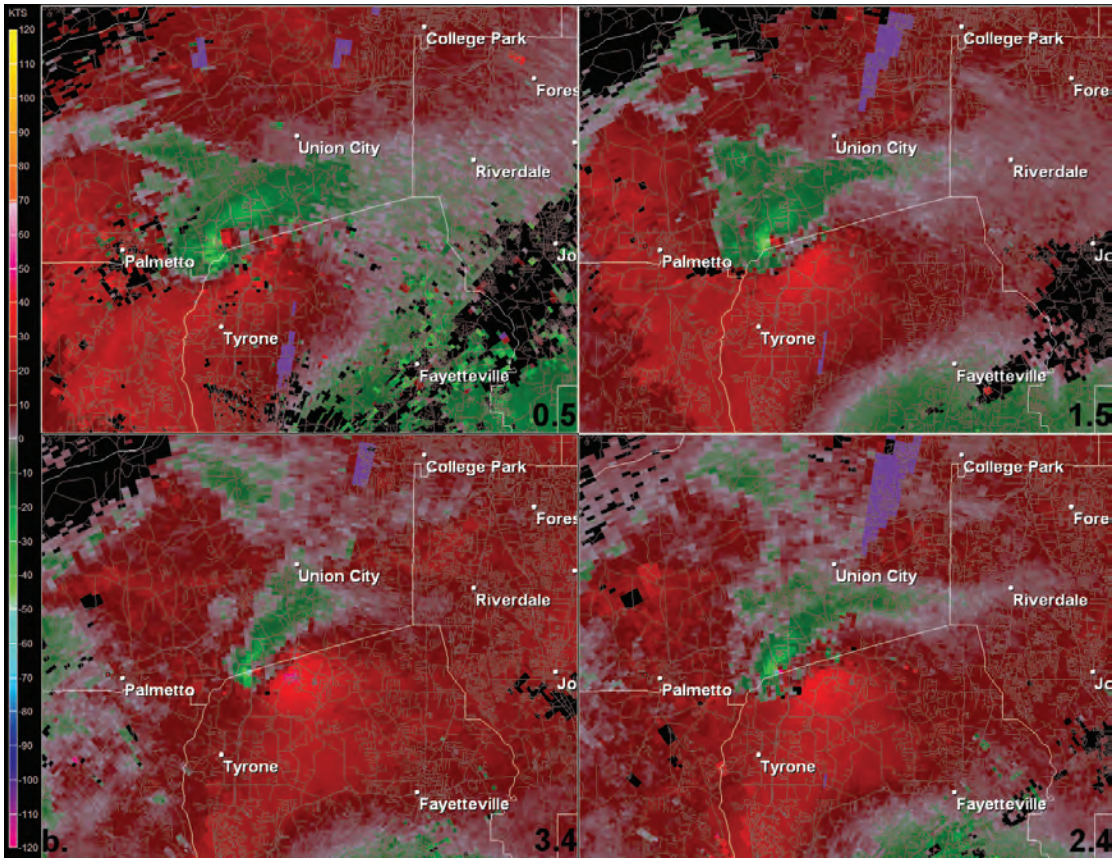

Fig. 11. GR2Analyst (a) reflectivity and (b) storm-relative velocity image from KFFC of supercell S1 at 2156 UTC as it produced F2 damage near the community of Tyrone in northern Fayette County. Clockwise from upper left in both images: 0.5°, 1.5°, 2.4°, and 3.4°.

Fig. 12-a

Fig. 12-b

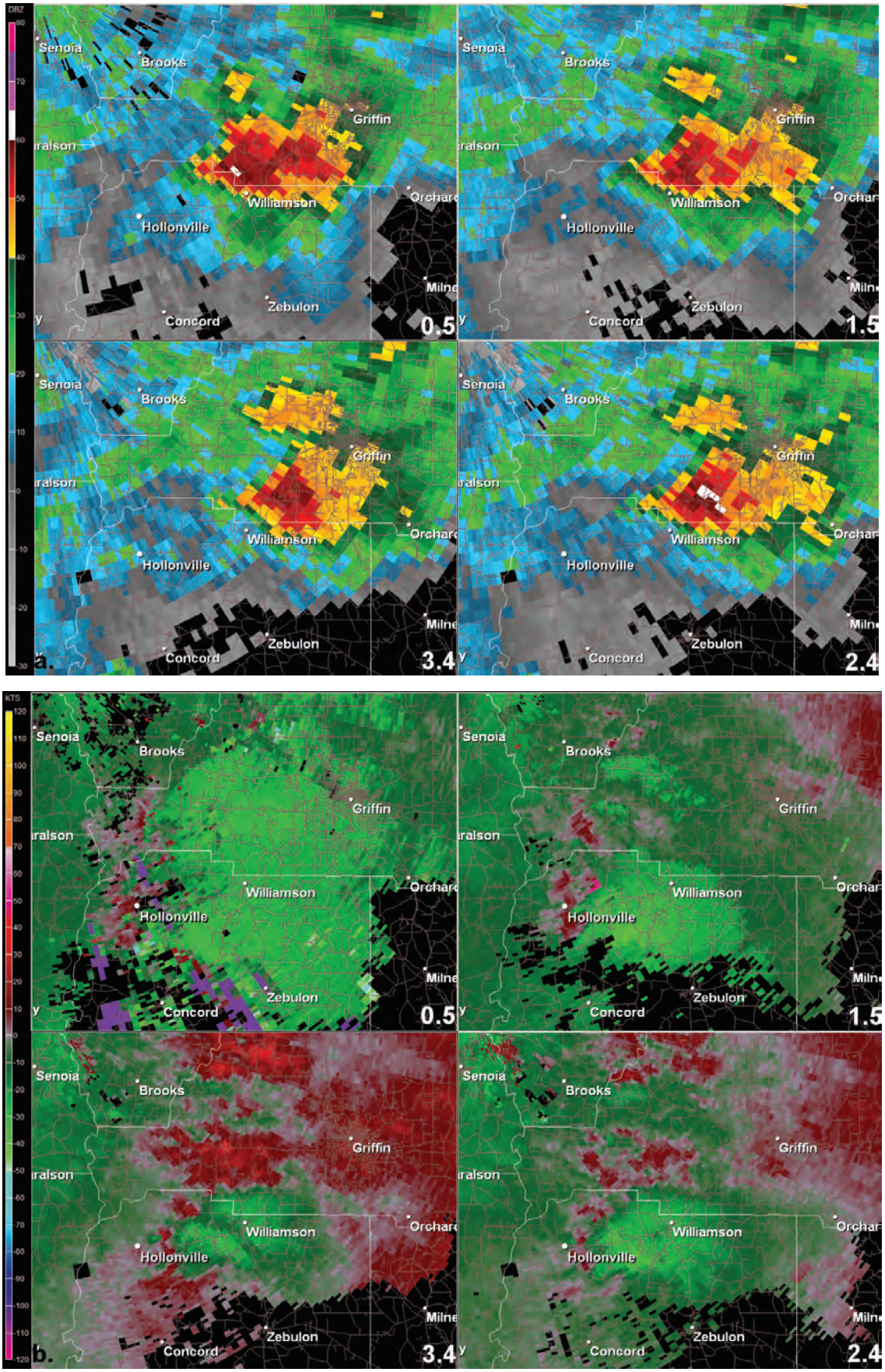

Fig. 12. GR2Analyst (a) reflectivity and (b) storm-relative velocity image from KFFC of supercell S8 at 2212 UTC as the tornado touched down near the community of Hollonville in northwest Pike County. Clockwise from upper left in both images: 0.5°, 1.5°, 2.4°, and 3.4°.

Fig. 13-a

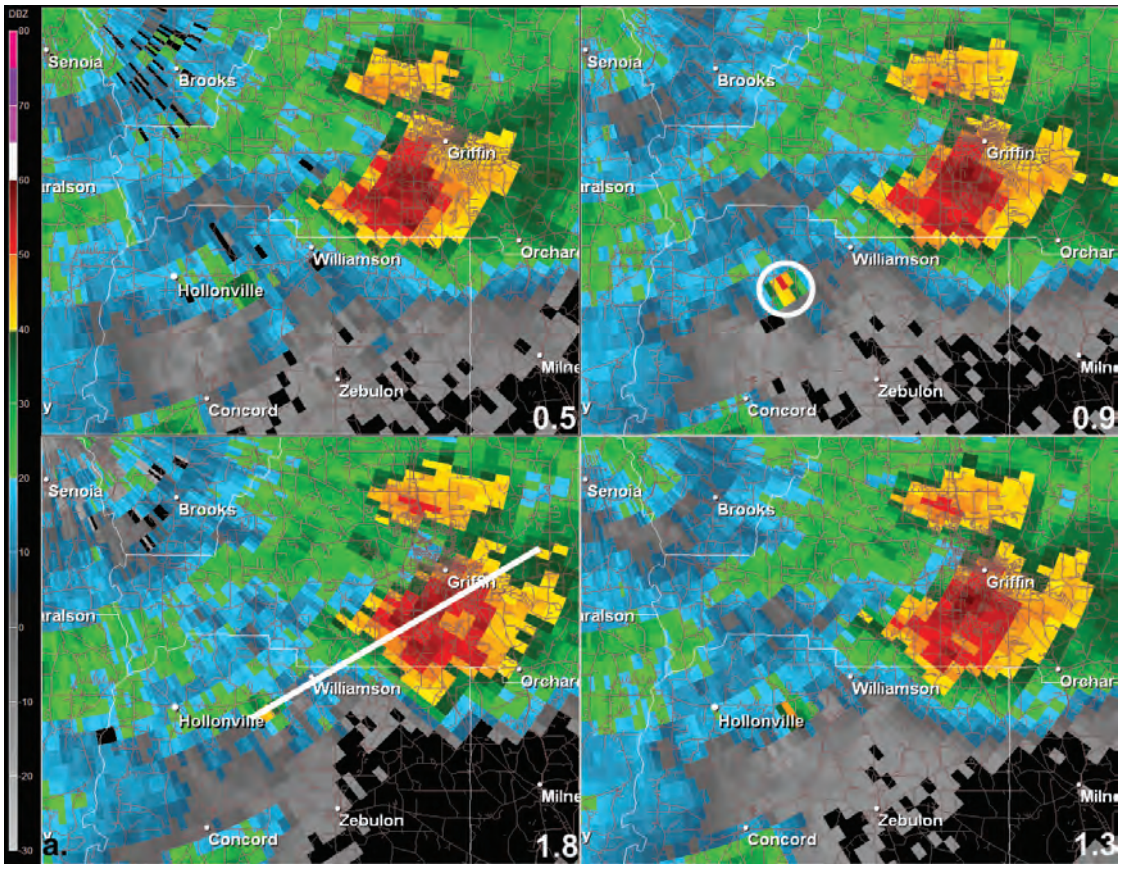

Fig. 13-b

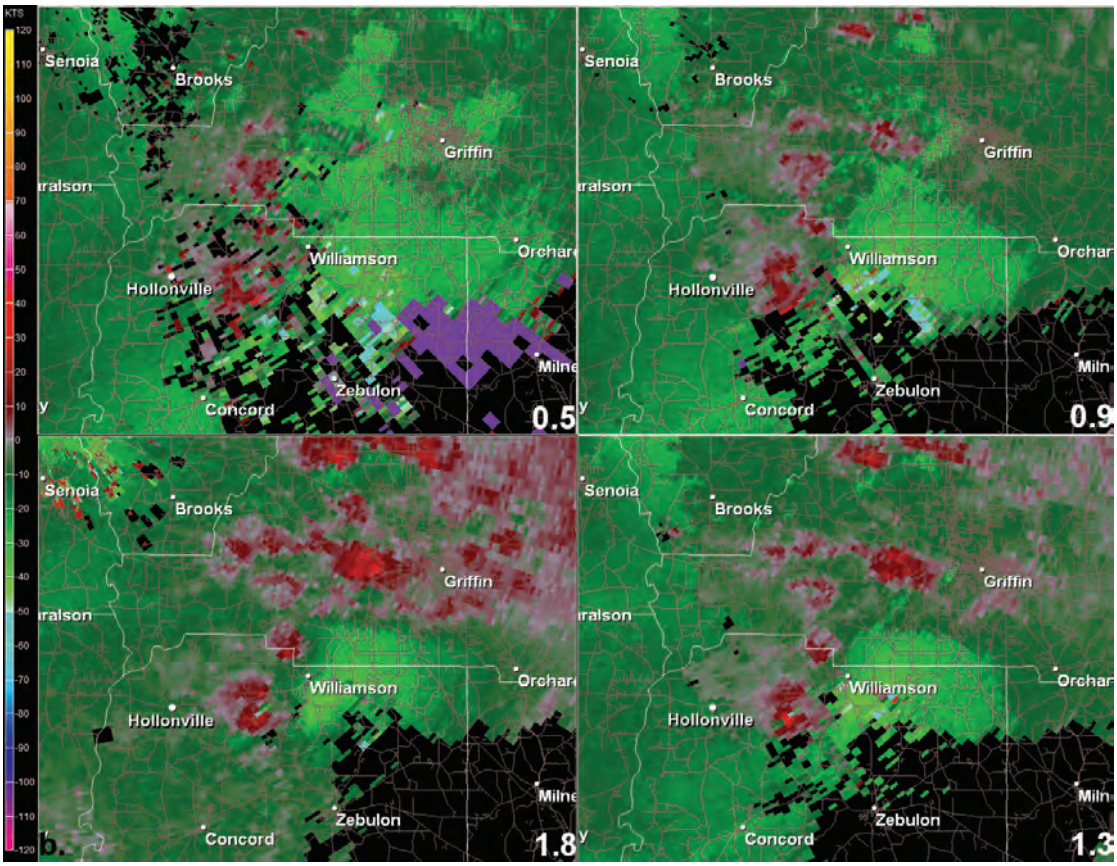

Fig. 13. GR2Analyst (a) reflectivity and (b) storm-relative velocity image from KFFC of storm S8 at 2218 UTC as it produced F3 damage near the community of Hollonville in northwest Pike County. Clockwise from upper left in both images: 0.5°, 0.9°, 1.3°, and 1.8°. The line on 1.8° indicates the location of the cross-section for Fig. 14.

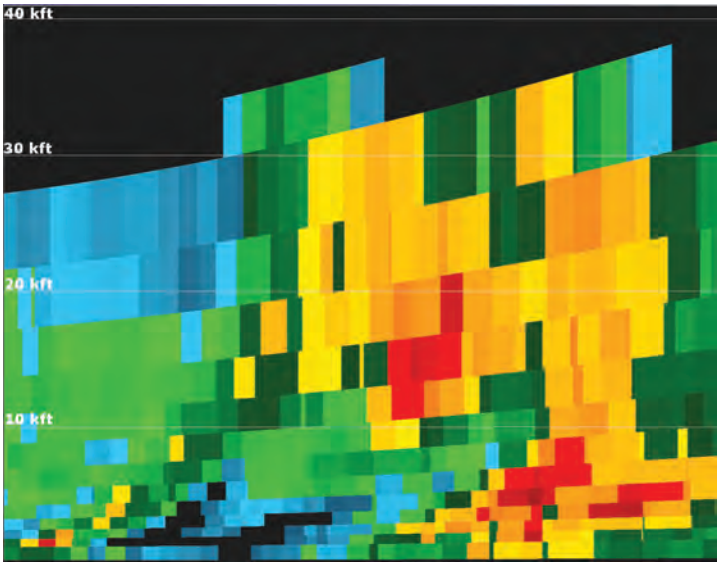

Fig. 14. GR2Analyst reflectivity cross-section from KFFC of S8 at 2218 UTC as the tornado touched down near the community of Hollonville in northwest Pike County.

one hour after the storm initiated, and approximately 30 minutes after the storm began rotating.

S1 did not show any signs of low-level rotation until 2113 UTC; this is one volume scan after the maximum reflectivity increased by about 10 dBZ, and the VIL increased substantially as well, from 25 g kg^{-1} to 45 g kg^{-1}. By 2123 UTC, an appendage on the southwest side of the storm clearly emerged, while reflectivity cores in the mid-levels of the storm exceeded 70 dBZ. On several consecutive scans after 2123 UTC and at multiple elevation angles, three body scatter spikes (TBSS), indicating the presence of large hail in the storm, were detected along radials beyond the storm. A final note for this volume scan was that just to the southwest of this storm, a thus-far nonsevere storm to the southwest split (this was the fourth volume scan in the splitting sequence). The right-mover (S2 – Fig. 1) would go on to produce hail in Newnan (Coweta County) and Peachtree City (Fayette County). The left-mover (S2'– Fig. 1), however, would travel north-northeast to impact and interact with S1 after 2145 UTC.

By 2134 UTC, the first hook echo emerged at the 0.5° slice, in extreme southwest Fulton County. By 2140 UTC, the reflectivities aloft in S2' to the southwest of S1 began to graze the back edge of the hook echo (not shown), and rotational velocities increased slightly at the 3.1° elevation scan. At 2145 UTC, 35-40 dBZ echoes from S2' can be seen to intersect the hook echo of S1, and low-level rotation increased significantly, with rotational velocity increasing by almost 14 kt, from 31.5 kt to 45.3 kt (with a 1 nm mesocyclone diameter) between this and the previous 0.5° scan. The first tornado of the day touched down at this same time, remaining on the ground from 2145-2156 UTC. As the storm was producing F2 damage in the community of Tyrone in northern Fayette County (Fig. 11), the left-mover that grazed the hook echo can clearly be seen, still traveling to the north-northeast, to the northwest of the tornadic supercell (i.e., this would be classified as a non-merger interaction, after Lee et al. 2006). By 2207 UTC, the tornado had lifted and only an appendage remained of the former hook echo, but the storm transitioned to HP (not shown) and remained severe for another 20 minutes, producing hail up to 1.75 inches. The storm would eventually interact with other storms (see below), but it eventually dissipated in more stable air just south of the wedge front. While not actually within the cold dome associated with the CAD, this area remained relatively stable due to persistent stratus clouds through the afternoon hours and had not destabilized as it did in areas to the south and southwest. [Note: Radar loops of S1 (both reflectivity and velocity) are online at http://www.srh.noaa.gov/ffc/html/tor010206b.shtml.]

As mentioned above, tornadogenesis occurred as S2' grazed the hook echo of S1. It is possible that precipitation loading from anvil hydrometeors or evaporative cooling underneath the anvil of S2' contributed to the descent needed to allow the rear-flank downdraft (RFD) to form, thereby allowing for near-simultaneous tightening and lowering of the mesocyclone (Markowski 2002). However, Markowski et al. (2002) seem to indicate that evaporational cooling and/or entrainment of mid-level cool air is not as important as previously thought, in regards to tornadic supercells. Without sufficient observations or model simulations of the storm, it is impossible to know if this was the case. The fact that tornadogenesis occurred just as S2' contacted S1, however, does raise the question as to whether or not tornadogenesis would have occurred without this series of events.

b. Supercell S8

Although S8 produced the strongest tornado of the day (an F3 resulting in three injuries), its structure and evolution were significantly different from the CL supercell S1. Using the same thresholds as with S1, the first discernible echo associated with S8 appeared at 2102 UTC. Similar to S1, the F3 tornado in S8 touched down approximately one hour after the storm initiated; however the striking difference was in the evolution of the two storms, most notably the lack of a coherent mesocyclone in S8. The storm developed approximately 25 km southeast of the main line of convection and was characterized by much lower reflectivity values through initial tornadogenesis. This is in agreement with the finding of Bluestein and Parks (1983) that LP storms form as isolated cells, "often to the south of a broken line of existing storms;" and were supercells in this case.

By 2207 UTC, just before tornadogenesis, VIL values in S8 finally climbed to 40 g kg^{-1} (Fig 10); this was the strongest this storm had been thus far. (Notice that at the same time, relative to the tornado event, S1 was rapidly weakening.) Weak rotation had also been detected, but was not collocated with S8; that is, the rotation appeared detached from the storm itself. No other well-defined rotation was evident with this storm prior to tornadogenesis. The short-lived F3 tornado touched down at 2212 UTC and traveled east across Pike County roughly during two volume scans (Figs. 12 and 13), lifting at 2218 UTC. No hook echo or appendage from the main cell was evident, even in reflectivity data aloft. The small area of 50 dBZ at 0.9° at 2218 UTC in Fig. 13a (notated) is likely tornado debris, acting as scatterers. Very weak reflectivity values, on the order of 10-15 dBZ are all that exist as a connection between the area of tornado debris and the forward-flank downdraft (FFD) in lower elevation scans (in fact, the first true hook echo emerged from S8 at 0.5° between 2235-2240 UTC). Using the cross-section analysis of reflectivity at 2218 UTC, however, a narrow axis of 30 to 50 dBZ returns is apparent extending upward from the low-level reflectivity associated with the tornado debris to the elevated higher reflectivity with the FFD (Fig. 14). Note the 5 nm area of little or no reflectivity from the surface to 5000 ft AGL from near the location of the tornado debris to the FFD.

Strong rotation was evident only for the 2216 UTC scan at 0.5° from KJGX (not shown), located near Warner Robbins Air Force Base (approximately 118 km southeast of S8), with rotational velocity of 45 kt. However, the approximate elevation of the 0.5° radar beam from KJGX was over 5500 ft AGL, whereas KFFC's was less than 1000 ft AGL. Reflectivity from KJGX also did not show a hook echo or a well-defined connection between the low-level rotation and the FFD.

A Pike County Sheriff's Deputy captured the bulk of the tornado's life cycle on camera, and through this medium, the clear slot from the RFD and much of the exposed updraft of the storm can clearly be seen. Near the beginning of the tornado's life, multiple vortices were observed near the surface. As the tornado intensified, a significant amount of debris can be seen, accounting for the reflectivity "ball" in Figs. 13 and 14. At all times during the video, the view remained virtually precipitation-free. This visual lack of precipitation around the tornado confirmed the lack of reflectivity on radar and seemingly confirmed the hypothesis that initially, the storm began as an LP supercell. However, attesting to the transitional nature of the supercell, VIL began increasing around tornadogenesis (Fig. 10), and once the tornado dissipated, updrafts increased rapidly in the storm as shown by the trends in echo tops. S8 quickly became an HP supercell before producing subsequent tornadoes.

At approximately 2130 UTC, a shower to the southwest of S8 developed and began moving northeast, into the inflow of S8. The shower was fully ingested in S8's weak echo region (WER) at the radar scan beginning at 2212 UTC – just as tornadogenesis was believed to have occurred. The shower can barely be discerned south of the FFD at the 0.5° elevation angle in Fig. 12. As with S1, it is possible that precipitation loading from this merger provided the downdraft necessary to tilt horizontal vorticity and produce large vertical vorticity values at the surface in order to lead to tornadogenesis (Markowski 2002). [Note: Radar loops of S8 (both reflectivity and velocity), as well as a link to the video of the tornado, are available online at http://www.srh.noaa.gov/ffc/html/tor010206b.shtml.]

With both S8 and S1, the conclusions found by Lee et al. (2006) are highly applicable. Although their analysis involved only a single outbreak, they found that tornadoes were associated with 57% of mergers that involved supercells. As such, they concluded that special attention should be paid to storm mergers as they could be an indicator of "heightened tornado threat, especially when the background storm environment features high relative humidity and [lifting condensation levels] LCLs…" For the 2 January event, 100 mb mixed layer lifting condensation levels (MLLCLs) were at or below 600 m AGL until dryline passage (not shown). In the Craven et al. (2002) study, they found that the median value of MLLCL for significant tornadoes was between 750 and 1000 m, thus the 2 January case was most certainly characterized by low LCLs, and surface data indicated high relative humidity. Lee et al. (2006) also recommended the identification of "developing weaker cells whose anticipated paths could intersect the projected position of a preexisting supercell…" as "there exists at least circumstantial evidence that subsequent cell mergers with a supercell may prompt cyclic tornadogenesis." This describes the situation with S8 very well; as it eventually evolved into more of an HP supercell, going on to produce three more tornadoes (two F1s and an F0) after the tornado near Hollonville.

The observations from 2 January 2006 and S8 in particular, also support the hypothesis set forth in Wurman et al. (2007). They suggest that a storm merger can enhance or trigger tornadogenesis by increasing the stretching of low-level vertical vorticity. In addition, by introducing rain-cooled air into the updraft, the merger can then subsequently disrupt that same stretching mechanism, thereby hastening the dissipation process, possibly resulting in short-lived tornadoes.

Conclusions

The unique near-storm environment in North Georgia on 2 January 2006, consisting of an unusually high θ_e January airmass, cold-air damming beginning to erode, an approaching dryline, splitting storms and storm mergers, combined with strong synoptic forcing allowed for an atypical wintertime outbreak in which supercells crossed the spectrum of classifications. In comparing the lifecycles of supercells S1 and S8 as they produced the two most significant tornadoes of the day, the differences between the two are profound.

S1, which developed along the dryline, developed as a classic (CL) supercell, with typical mesocyclone structure. The mesocyclone tightened and tornadogenesis occurred as S2' (Fig. 1) grazed the back edge of the hook echo. The tornado, rated an F2 on the legacy Fujita scale, was on the ground for 17 minutes (2145-2202 UTC) as it traveled its 11 km path. The storm eventually evolved into an HP supercell as it continued to produce hail and damaging winds downstream. It was even involved with yet another storm merger and subsequent weak tornado (see below), but as it moved into a far more stable environment east of the Atlanta Metro area, the storm eventually dissipated.

S8, unlike S1, developed approximately 25 km ahead of the dryline, thus placing it in a region that had not been contaminated by surrounding convection. S8 showed characteristics of an LP supercell during the early part of its life. However, similar to S1 at the time of tornadogenesis, it too interacted with another cell, but this shower crossed the storm's inflow and was eventually ingested into the larger cell's WER. The tornado produced by this storm, rated as an F3 on the legacy Fujita scale, was on the ground for six minutes as it traveled its 5 km path. Beginning as an LP supercell, the storm spanned the supercell spectrum during its long and cyclic life, briefly evolving into a CL and eventually into a long-lived HP supercell, from which additional tornadoes developed, all of which were initiated by storm mergers or interactions.

While these two storms produced the most significant tornadoes of the day, there were other supercells that developed later in the evening that produced an additional four tornadoes. Each subsequent tornado, much like the two preceding them, was the result of a storm merger or non-merger interaction of some sort. An F1 tornado was produced from a supercell resulting from a three-storm interaction: the left-moving S8' merged with the weak remains of S1, the combination of which then interacted with the weak remains of S2, a non-tornadic supercell. The other three tornadoes (two F1s and an F0) all touched down from storms that followed from the remnants of S8. These tornadoes developed when the storm was interacting and/or merging with another storm. By the time the last tornado occurred, the storm had merged with another storm and had deviated significantly to the right, moving in an east-southeasterly direction.

This set of storms and the relationships between them demonstrate how complex the nature of supercell storm evolution and tornadogenesis can become. Storm splits, mergers, and interactions took place within the unique evolution of at least two distinctly different supercell storm lifecycles. However, it seems clear from the data that in this event, each tornado occurred as a result of either a cell merger or at least non-merger interaction. While it may be difficult for warning forecasters to catch these interactions in real-time, it is crucial that meteorologists' situational awareness be heightened when these types of occurrences are possible.

Acknowledgments

Student participation for B. Miller was funded by the 2006 NOAA/Earnest F. Hollings Scholarship program. The authors would like to thank Dr. Christopher Weiss of Texas Tech University for his insights regarding dryline evolution and propagation. Thanks also to Dan Darbe, Michael Griesinger, and Gary Beeley (retired) in particular, as well as to several other current and former meteorologists at the Weather Forecast Office (WFO) Peachtree City for their help and support throughout this study. In addition, we would like to acknowledge Jeff Evans, Rich Thompson, and David Imy from the SPC, Les Lemon from the National Weather Service (NWS) Warning Decision Training Branch, Kevin Pence from WFO Birmingham, AL, and Matt Bunkers from WFO Rapid City, SD, for their insights and expertise relevant to this event. Wendy Moen from WFO Charleston, SC, is also recognized for her assistance with respect to CAD erosion. Finally, we would like to thank reviewers Stephen Jascourt and Christopher Buonanno for their helpful comments and suggestions.

Mention of a proprietary product or service does not imply endorsement thereof by the authors or NOAA/NWS. Such references are provided only to fully inform the reader of the resources used in the performance of the work reported.

Authors

Trisha D. Palmer is a General Forecaster at WFO Peachtree City, GA, a position she has held since 2005. Her previous positions include: Intern at WFO Raleigh, NC; student intern at WFO Raleigh, NC; and student intern at WFO Little Rock, AR. She received a Master of Science degree in Atmospheric Science in 2004 from North Carolina State University and a Bachelor of Science degree in Meteorology in 2002 from the University of Oklahoma. Her meteorological interests are wide-ranging, from severe convection, to winter weather (especially CAD), to hydrology. She especially enjoys science sharing, training, and working with students. She is married to a meteorologist, Joshua Palmer, a Hydrometeorological Analysis and Support Forecaster at the Southeast River Forecast Center

Brandon A. Miller is a meteorologist and weather producer for CNN International in Atlanta, where he covers major weather stories from around the world. He began his career with CNN as an intern in 2004. He received a Master of Science degree in Earth and Atmospheric Science from the Georgia Institute of Technology in 2008, and received a Bachelor of Science degree in Earth and Atmospheric Science in 2006, also from Georgia Tech. He conducted research for this project as part of the NOAA/Ernest F. Hollings Scholarship, which he received in 2005/2006. Brandon was also a National Weather Center Research Experience for Undergraduates (REU) student in Norman, Oklahoma in 2005, where he developed a passion for storm chasing. His other interests, outside of weather, include playing golf and spending time at the beach.

Lans P. Rothfusz is the Meteorologist in Charge of the National Weather Service's (NWS) Weather Forecast Office in Peachtree City, Georgia. He earned his Bachelor of Science degree in Meteorology from the University of Wisconsin-Madison (1982) and his Master of Science degree in Meteorology from the University of Oklahoma (1985). After two years of postgraduate work at the University of Oklahoma, he began his tenure with the NWS in 1987. With the NWS, he has served in Chattanooga, Tennessee; Oklahoma City, Oklahoma; Fort Worth, Texas; as Deputy Meteorologist in Charge of the Peachtree City, Georgia office; and then the Meteorologist in Charge of the offices in Tulsa, Oklahoma and now Peachtree City, Georgia.

Steven E. Nelson is the Science and Operations Officer at the NOAA/NWS WFO in Peachtree City, Georgia since 2007. He earned his Bachelor of Science and Master of Science degrees in Meteorology, both from the University of Oklahoma, in 1991 and 1994, respectively. Steve served as Meteorologist Intern at the Norman, Oklahoma WFO, Journeyman Forecaster at the Tulsa, Oklahoma WFO, Information Technology Officer at the Norman WFO, and as Lead Forecaster at the Peachtree City WFO. His meteorological interests include severe convection and improving forecaster situational awareness prior to high impact events.

References

Bailey, C. M., G. Hartfield, G. M. Lackmann, K. Keeter, and S. Sharp, 2003: An objective climatology, classification scheme, and assessment of sensible weather impacts for Appalachian cold-air damming. *Wea. Forecasting*, 18, 641-661.

Barbré, R. E., Jr., J. Mecikalski, K. Knupp, W. Mackenzie, Jr., P. Gatlin, and D. Phillips: 2005: An observational analysis of an Alabama dryline event on March 19-20, 2003. Preprints, *21st Conf. on Weather Analysis and Forecasting*, Washington, D.C., Amer. Meteor. Soc., CD-ROM, P1.15.

Bell, G. D., and L. F. Bosart, 1988: Appalachian cold-air damming. *Mon. Wea. Rev.*, 116, 137–161.

Bluestein, H. B., and C. R. Parks, 1983: A synoptic and photographic climatology of low-precipitation severe thunderstorms in the southern plains. *Mon. Wea. Rev*, 111, 2034–2046.

_____, and G. R. Woodall, 1990: Doppler-radar analysis of a low-precipitation (LP) severe storm. *Mon. Wea. Rev.,* 118**,** 1640–1664.

Bosart, L. F., 1975: New England coastal frontogenesis. *Quart. J. Roy. Meteor. Soc.,* 101**,** 957–978.

Brennan, M. J., G. M. Lackmann, and S. E. Koch, 2003: An analysis of the impact of a split-front rainband on Appalachian cold-air damming. *Wea. Forecasting*, 18, 712-731.

Businger, S., W. H. Bauman III, and G. F. Watson, 1991: The development of the Piedmont front and associated outbreak of severe weather on 13 March 1986. *Mon. Wea. Rev.*, 119, 2224–2251.

Craven, J. P., H. E. Brooks, and J. A. Hart, 2002: Baseline climatology of sounding derived parameters associated with deep, moist convection. Preprints, *21st Conf. on Severe Local Storms,* San Antonio, TX, Amer. Meteor. Soc., 643–646.

Davies, J. M., and R. H. Johns, 1993: Some wind and instability parameters associated with strong and violent tornadoes. Part I: Wind shear and helicity. *The Tornado: Its Structure, Dynamics, Prediction, and Hazards, Geophys. Monogr*., No. 79, Amer. Geophys. Union, 573-582.

Davies-Jones, R. P., D. Burgess, and M. Foster, 1990: Test of helicity as a tornado forecast parameter. Preprints, *16th Conf. on Severe Local Storms,* Kananaskis Park, AB, Canada, Amer. Meteor. Soc., 588–592.

Doswell, C. A., III, and D. W. Burgess, 1993: Tornadoes and tornadic storms: A review of conceptual models. *The Tornado: Its Structure, Dynamics, Prediction, and Hazards, Geophys. Monogr.,* 79, Amer. Geophys. Union, 161–172.

_____, A. R. Moller, and R. W. Przybylinski, 1990: A unified set of conceptual models for variations on the supercell theme. Preprints, *16th Conf. on Severe Local Storms,* Kananaskis Park, AB, Canada, Amer. Meteor. Soc., 40–45.

Guyer, J. L., D. A. Imy, A. Kis, and K. Venable, 2006: Cool season significant (F2-F5) tornadoes in the Gulf Coast States. Preprints, *23d Conf. Severe Local Storms*, St. Louis MO., Amer. Meteor. Soc., CD-ROM, 4.2.

Hane, C. E., C. L. Ziegler, and H. B. Bluestein, 1993: Investigation of the dryline and convective storms initiated along the dryline: Field experiments during COPS-91. *Bull. Amer. Meteor. Soc.,* 74**,** 2133–2145.

_____, M. E. Baldwin, H. B. Bluestein, T. M. Crawford, and R. M. Rabin, 2001: A case study of severe storm development along a dryline within a synoptically active environment. Part I: Dryline motion and an Eta Model forecast. *Mon. Wea. Rev.*, 129, 2183–2204.

Johns, R. H., J. M. Davies, and P. W. Leftwich, 1993: Some wind and instability parameters associated with strong and violent tornadoes. Part II: Variations in the combinations of wind and instability parameters. *The Tornado: Its Structure, Dynamics, Prediction, and Hazards*. *Geophys. Mongr*., 79, Amer. Geophys. Union, 583-590.

Keeter, K. K., S. Businger, L. G. Lee, and J. S. Waldstreicher, 1995: Winter weather forecasting throughout the eastern United States. Part III: The effects of topography and the variability of winter weather in the Carolinas and Virginia. *Wea. Forecasting*, 10, 42–60.

Lackmann, G. M., and W. M. Stanton, 2004: Cold-air damming erosion: Physical mechanisms, synoptic settings, and model representation. Preprints, *20th Conf. on Weather Analysis and Forecasting*, Seattle, WA, Amer. Meteor. Soc., CD-ROM, 8.3.

Lee, B. D., B. F. Jewett, and R. B. Wilhelmson, 2006: The 19 April 1996 Illinois tornado outbreak. Part II: Cell mergers and associated tornado incidence. *Wea. Forecasting*, 21, 449-464.

Maddox, R. A., 1976: An evaluation of tornado proximity wind and stability data. *Mon. Wea. Rev.*, 104, 133-142.

Markowski, P. M., 2002: Hook echoes and rear-flank downdrafts: A review. *Mon. Wea. Rev.*, 130, 852–876.

_____, J. M. Straka, and E. N. Rasmussen, 2002: Direct surface thermodynamic observations within the rear-flank downdrafts of nontornadic and tornadic supercells. *Mon. Wea. Rev*., 130, 1692-1721.

Moller, A. R., C. A. Doswell III, M. P. Foster, and G. R. Woodall, 1994: The operational recognition of supercell thunderstorm environments and storm structures. *Wea. Forecasting*, 9, 327–347.

Moore, J. T. and G. E. VanKnowe, 1992: The effect of jet-streak curvature on kinematic fields. *Mon. Wea. Rev.*, 120, 2429-2441.

Rasmussen, E. N., and D. O. Blanchard, 1998: A baseline climatology of sounding-derived supercell and tornado forecast parameters. *Wea. Forecasting*, 13, 1148–1164.

Rhea, J. O., 1966: A study of thunderstorm formation along drylines. *J. Appl. Meteor.,* 5**,** 58–63.

Richwein, B. A., 1980: The damming effect of the southern Appalachians. *Natl. Wea. Dig.*, 5(1), 2–12.

Schumacher, P. N., D. J. Knight, and L. F. Bosart, 1996: Frontal interactions with the Appalachian Mountains. Part I: A climatology. *Mon. Wea. Rev.*, 124, 2453–2468.

Stanton, W. M., 2003: An analysis of the physical processes and model representation of cold air damming erosion. M.S. thesis, Dept. of Marine, Earth, and Atmospheric Sciences, North Carolina State University, 224 pp.

Thompson, R. L., R. Edwards, J. A. Hart, K. L. Elmore, and P. Markowski, 2003: Close proximity soundings within supercell environments obtained from the Rapid Update Cycle. *Wea. Forecasting*, 18, 1243-1261.

_____, _____, and C. M. Mead, 2004: An update to the supercell composite and significant tornado parameters. Preprints, *22d Conf. Severe Local Storms*, Hyannis MA, Amer. Meteor Soc., CD-ROM, 8.1.

U.S. Dept. of Commerce, 2006: *Storm Data*, Vol. 48, No. 1, NOAA, NESDIS, NCDC, 182 pp. [Available from the National Climatic Data Center, 151 Patton Ave., Asheville, NC 28801-5001].

Vescio, M. D., K. K. Keeter, G. Dial, P. Badgett, and A. J. Riordan, 1993: A low-top reflectivity severe weather episode along a thermal/moisture boundary in eastern North Carolina. Preprints, *17th Conf. on Severe Local Storms,* St. Louis, MO, Amer. Meteor. Soc., 628–632.

Wurman, J. M., Y. P. Richardson, C. Alexander, S. Weygant, P. F. Zhang, 2007: Dual-Doppler and single-Doppler analysis of a tornadic storm undergoing mergers and repeated tornadogenesis. *Mon. Wea. Rev*., 135, 736-758.

Zittel, W. D., and T. Wiegman, 2005: VCP 121 and the Multi-PRF Dealiasing Algorithm. *NEXRAD Now*, 14, 9-15.